Biosensors and Bioelectronics 141 (2019) 111403

Contents lists available at ScienceDirect

Biosensors and Bioelectronics

journal homepage: www.elsevier.com/locate/bios

Peptide-functionalized upconversion nanoparticles-based FRET sensing platform for Caspase-9 activity detection in vitro and in vivo

Lin Liu[a,b], Hua Zhang[b,*], Zhenxin Wang[b], Daqian Song[a,**]

[a] College of Chemistry, Jilin University, Changchun, 130012, PR China
[b] State Key Laboratory of Electroanalytical Chemistry, Changchun Institute of Applied Chemistry, Chinese Academy of Sciences, Changchun, 130022, PR China

ARTICLE INFO

Keywords:
Fluorescence resonance energy transfer biosensor
Peptide modified upconversion nanoparticle
Caspase-9 activity
Upconversion luminescence imaging

ABSTRACT

In the present work, peptide-functionalized upconversion@silica nanoparticle (termed as UCNP@SiO_2@Cy5-pep)-based fluorescence resonance energy transfer (FRET) sensing platform has been fabricated for the detection of caspase-9 activity in vitro and in vivo. A Cy5 labeled peptide containing specific motif LEHD for caspase-9 cleavage was designed and conjugated with UCNP@SiO_2 through covalent attachment. The red upconversion luminescence (UCL) emission of UCNP@SiO_2 can be quenched by Cy5 while the green UCL emission of UCNP@SiO_2 remains undisturbed. After the cleavage of LEHD by caspase-9, the Cy5 departed from UCNP@SiO_2 surface, resulting in recovery of red UCL emission of UCNP@SiO_2. The UCNP@SiO_2@Cy5-pep has been successfully used to monitoring the changes of caspase-9 activity levels in apoptotic cancerous cells (MG-63 and SW480) by cisplatin-induction. Under same experimental conditions, it is found that the intracellular caspase-9 activity level of cisplatin-treated MG-63 cells is higher than that of cisplatin-treated SW480. This result is consistent with that of commercial caspase-9 activity kits. The UCL signal intensity ratio of red emission to green emission of UCNP (termed as R/G) is linearly dependent on the amount of MG-63 cells within the range of 5×10^3 to 1×10^6 cells (i.e., 0.5–100 U mL^{-1} caspase-9) with a limit of detection (LOD) of 675 cells (i.e., 0.068 U mL^{-1} caspase-9). Furthermore, the practicability of UCNP@SiO_2@Cy5-pep is demonstrated by detection of caspase-9 activities in tumor tissues in vivo, and satisfactory results are obtained.

1. Introduction

Apoptosis is an evolutionarily conserved form of cell suicide that requires specialized mechanisms. The central component of this machine is a proteolytic system involving a series of proteases called caspases. These enzymes are involved in a cascade that triggers and eventually forms in response to a pro-apoptotic signal, culminates in cleavage of a set of proteins, and finally leads to cell disassembly (Hurtley, 2016; Johnstone et al., 2002; Poreba et al., 2015; Vaux and Korsmeyer, 1999). Caspase-9, a prominent member of caspase family, is a key activator of the caspase cascade, which is implicated in apoptosis and cytokine processing (Mehmet, 2000). Activated caspase-9 further initiates the proteolytic activities of other downstream caspases, which degrade a variety of substrates and result in cell disassembly and cell death ultimately (Deveraux et al., 1998; MacFarlane et al., 1997; Sun et al., 1999). Therefore, the real-time monitoring of caspase-9 activity in vivo is of great significance for the prognosis of diseases and the development of anti-cancer drugs (Sun et al., 1999). A number of methods have already been developed for in vitro and in vivo detection of caspase-9 including the enzyme-linked immune sorbent assay (ELISA), Western blot analysis, electrochemical biosensors, fluorescence resonance energy transfer (FRET)-based assays (Hakem et al., 1998; Prokhorova et al., 2018; Shieh et al., 2019; Suzuki et al., 2015; Thamizharasi et al., 2019; Tian et al., 2019). However, conventional organic fluorescent probes often suffer from short fluorescence life time, short excitation wavelengths and poor photostability (Shi et al., 2015), which could reduce both in vivo imaging penetration depth and sensitivity. Developing novel sensing platforms for in vivo detection of caspase activity is still highly challenging.

Upconversion nanoparticles (UCNPs) are a special class of lanthanide-doped nanoparticles that are able to convert near-infrared (NIR) light into higher-energy and multicolor UV/visible emission light (Park et al., 2015). With the multiple advantages of deep penetration, robust photostability, low toxicity, and minimal autofluorescence background in biological tissues (Achatz et al., 2011; Chen and Zhao, 2012), UCNPs are rapidly emerging as strong contenders for the traditional

* Corresponding author.
** Corresponding author.
E-mail addresses: zhanghua@ciac.ac.cn (H. Zhang), songdq@jlu.edu.cn (D. Song).

https://doi.org/10.1016/j.bios.2019.111403
Received 12 April 2019; Received in revised form 22 May 2019; Accepted 1 June 2019
Available online 03 June 2019
0956-5663/

downconversion-based fluorescence nanoparticles/fluorescence dyes in biosensor construction (Alonso-Cristobal et al., 2015; Zheng et al., 2015; Zhu et al., 2017). Moreover, UCNPs have been demonstrated as efficient FRET donors for various bioanalytical and biomedical applications (Chen et al., 2013; Lin et al., 2013; Wu et al., 2013). Since Wang et al. reported the first FRET biosensor based on 50 nm $Na(Y^{1.5}Na^{0.5})F_6$:Yb^{3+},Er^{3+}/Tm^{3+} UCNPs (the donor) and gold nanoparticles (the acceptor) in 2005 (Yuan et al., 2014), UCNP-based FRET systems have been extensively used to detect various analytes such as metal ions, DNA, biomolecules, and enzymes (Alonso-Cristobal et al., 2015; Kerr and de la Rica, 2015; Wang et al., 2016; Wang et al., 2010a; Zheng et al., 2015). For obtaining UCNPs with high fluorescence quantum yield and low nanocrystal defect, UCNPs are normally synthesized in organic phase. Several strategies including ligand exchange, silica coating, or small molecular surfactant wrapping have been used to transfer hydrophobic UCNPs into aqueous medium (Achatz et al., 2011; Chen and Zhao, 2012). In particular, SiO_2 coated UCNPs (UCNP@SiO_2) exhibit high biocompatibility, excellent optical property, good colloidal stability and facility of surface modification (Hu et al., 2009; Jiang and Zhang, 2010; Qiao et al., 2012; Wang et al., 2009).

Herein, a simple FRET sensing platform based on peptide-functionalized UCNP@SiO_2 has been fabricated for the detection of caspase-9 activity both of in vitro and in vivo. The FRET sensing platform is comprised of UCNPs as the energy donor and Cy5 with a high quantum yield (c.a. 28% (Mujumdar et al., 1993),) as the energy acceptor. In proof of the sensing principle, the FRET sensing platform is applied for detecting caspase-9 activity in two cancer cell lines under different culture conditions. Importantly, the cisplatin-induced enhancement of caspase-9 activity in vivo is successfully visualized by the proposed FRET sensing platform.

2. Experimental section

2.1. Materials and reagents

Lanthanide oxides (Gd_2O_3, Y_2O_3, Er_2O_3 and Yb_2O_3, 99% purity) and 1-ethyl-3-(3-dimethylaminopropyl) carbodiimide hydrochloride (EDC), were obtained from Alfa Aesar Co. (Ward Hill, USA). N-hydroxysulfosuccinimide sodium salt (sulfo-NHS) and cisplatin were obtained from Aladdin Reagent Ltd. (Shanghai, China). 1-octadecene (ODE, ≥90%), oleic acid (OA, ≥90%), Triton X-100 and tetraethylorthosilicate (TEOS, 99.999%) were purchased from Sigma-Aldrich Co. (St Louis, USA). Carboxyethylsilanetriol (CTES, sodium salt, 25% in water) was purchased from Leon Technology Ltd. (Beijing, China). NH_4F (analytical grade), 3-(4,5-dimethyl-2-thiazolyl)-2,5-diphenyl-2-H-tetrazolium bromide (MTT) and Dulbecco modified Eagle medium (DMEM) were supplied by Beijing Dingguo Biotechnology Ltd. (Beijing, China). Leibovitz's L-15 culture medium (L-15) were purchased from Jiangsu KenGen Biotech Ltd. (Jiangsu, China). Fetal bovine serum (FBS) and trypsin-EDTA cell detaching kit were purchased from Gibco Co. (New York, USA). SW480 and MG63 cell lines were purchased from Shanghai Cell Bank, CAS (Shanghai, China). The Cy5-modified peptide (Cy5-pep, sequence: CGRGGLEHDGGRK-Cy5) was synthesized by Synpeptide Ltd. (Shanghai, China). Caspase 9 inhibitor (Ac-LEHD-FMK) was purchased from Biovision Ltd. (Wuhan, China). Bradford protein quantitative kit was purchased from Bioteke Co. (Beijing, China). Caspase-9 activity colorimetric assay kit was obtained from BestBio Inc. (Shanghai, China). Other used reagents (analytical grade) were obtained from Beijing Chemical Reagents Co. (Beijing, China). Ultrapure water (18.2 MΩ cm) was prepared by Milli-Q system and used in all experiments.

2.2. Synthesis of Cy5-pep modified silica-coated UCNPs

The $NaYF_4$: Yb^{3+}, Er^{3+}@$NaGdF_4$ UCNPs and carboxyl-terminated silica-coated $NaYF_4$:Yb^{3+}, Er^{3+}@$NaGdF_4$ UCNPs (UCNP@SiO_2–COOH) were synthesized by a reported water-in-oil microemulsion method with slight modification (see supplementary information (SI) for details). The UCNP@SiO_2–COOH were dispersed in MES buffer (0.1 M, pH 6.0). 5 mL UCNP@SiO_2–COOH (1 mg mL^{-1}) was mixed with 0.5 mL EDC (2 mg mL^{-1} in MES buffer) and 0.5 mL sulfo-NHS (8 mg mL^{-1} in MES buffer), and stirred at room temperature for 1 h. The excessive EDC and sulfo-NHS were removed by repeated centrifugation (13000 rpm, 15 min, 3 times, 3 mL MES buffer), the precipitates were redispersed in 4 mL HEPES buffer (0.01 M, pH 7.4) containing different amounts of Cy5-pep (0.05, 0.1, 0.2, 0.4, 0.5 and 0.8 mg), respectively. The mixtures were stirred gently at room temperature for 3 h, respectively. Finally, Cy5-pep conjugated UCNP@SiO_2 (termed as UCNP@SiO_2@Cy5-pep) were purified by centrifugation at 4 °C (13000 rpm, 15 min, 3 times, 1 mL HEPES buffer) and resuspended in 1 mL HEPES buffer. For studying the biocompatibility of UCNP@SiO_2@Cy5-pep, the cytotoxicity of UCNP@SiO_2@Cy5-pep was evaluated by MTT assay, and the in vivo toxicity of UCNP@SiO_2@Cy5-pep was investigated by hematoxylin and eosin (H&E) staining and blood biochemistry assay (see SI for details).

2.3. Intracellular caspase-9 activity detection

The MG-63 and SW480 cells (1.5×10^5 cells per well) were cultured with 2 mL fresh DMEM or L-15 containing 10% FBS and 100 U mL^{-1} penicillin-streptomycin in 6-well microtiter plate under a humidified 5% CO_2 at 37 °C for 24 h, respectively. DMEM was used for culturing MG-63 cells, while L-15 was used for culturing SW480 cells. After washed with 1.5 mL PBS (3 times), the cells were cocultured with 200 μg mL^{-1} UCNP@SiO_2@Cy5-pep in 2 mL serum-free culture medium at 37 °C for another 4 h, respectively. The UCNP@SiO_2@Cy5-pep stained cells were washed with 1.5 mL cold PBS (3 times), and cocultured with various concentrations of cisplatin (0, 10, 20, 50 and 100 μM) in 2 mL culture medium at 37 °C for 12 h, respectively. Subsequently, the cisplatin treated cells were washed with 1.5 mL cold PBS (3 times), fixed with 4% paraformaldehyde for 20 min, and subjected to UCL imaging by a reconstructive Nikon Ti–S fluorescent microscope using a 980 nm continuous-wave (CW) NIR laser as excitation light source. The cells treated with Ac-LEHD-FMK (50 μM) and cisplatin (100 μM) were used as control samples. For UCL spectral measurements, UCNP@SiO_2@Cy5-pep stained cells were detached from 6-well plate using a commercial trypsin-EDTA cell detaching kit and centrifuged at 1000 rpm for 5 min. The cell precipitates containing different numbers of 100 μM cisplatin treated cells were redispersed in 1 mL PBS and measured on an F-4500 fluorescence spectrophotometer under an external 980 nm CW NIR laser excitation. For comparison, the caspase-9 activity assay kit was employed to detect the caspase-9 activity of MG-63 and SW480 cells stimulated by 100 μM cisplatin. The enzyme activities of 100 μM cisplatin treated MG-63 cells were also determined by the commercial caspase-9 activity colorimetric assay kit.

2.4. In vivo UCL imaging

All animal experiments were conformed to the guidelines of the Regional Ethics Committee for Animal Experiments established by Jilin University Institutional Animal Care and Use. BALB/c nude mice (4–6 weeks old, male) were purchased from Beijing HFK Biotechnology Ltd. (Beijing, China), which were injected subcutaneously with MG-63 cells and SW480 cells, respectively. The MG-63 and SW480 tumor-bearing nude mice were treated with cisplatin (5 mg kg^{-1} bodyweight) or saline through intratumoral injection when the volumes of tumors reached about 40 mm^3 at 21 days post-inoculation of cells. After 3 days, the mice were treated by the second dose of cisplatin or saline, respectively. The MG-63 tumor and SW480 tumor-bearing nude mice were injected intravenously with 200 μL 0.9 wt% NaCl solution containing 30 mg mL^{-1} UCNP@SiO_2@Cy5-pep at 2 days post-treatment of cisplatin/saline. The in vivo UCL images were collected at the appropriate

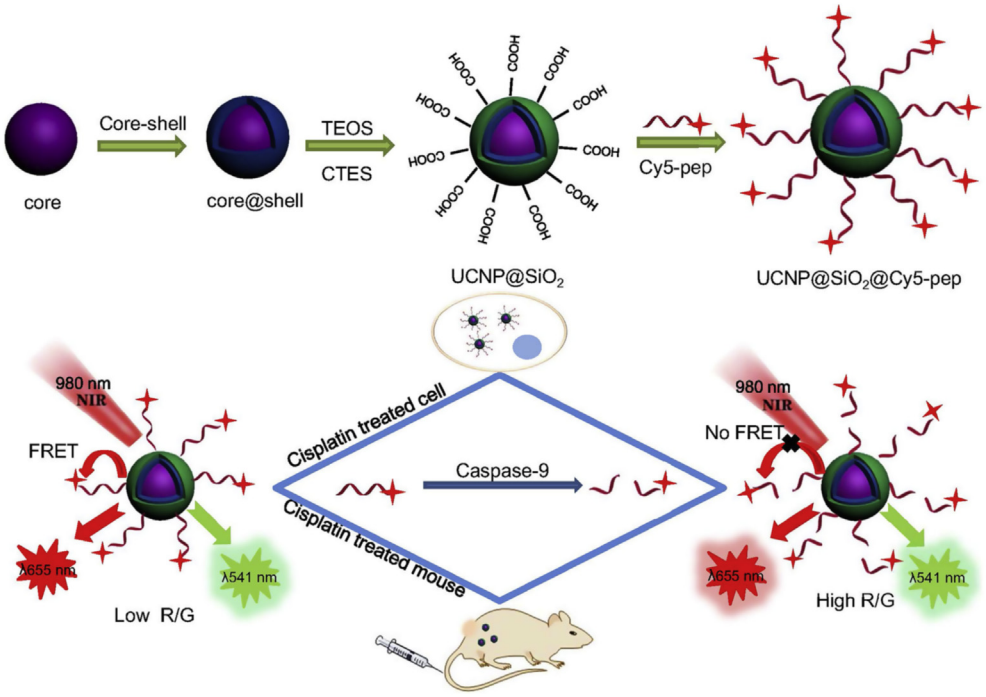

Sch. 1. The schematic representation of UCNP-based FRET sensing platform for the detection of caspase-9 activity both in vitro and in vivo.

time points of post-injection. The in vivo UCL images were recorded on a CCD camera under excitation of 980 nm CW NIR laser with the power density of 1.5 W cm^{-2} (see SI for details). The green and red emission intensity of each tumor was quantified using Image J software.

3. Results and discussion

3.1. Fabrication of the UCNP-based FRET sensing platform

As illustrated in Scheme 1, the UCNP-based FRET sensing platform was fabricated for the detection of caspase-9 activity, using UCNPs as the energy donor and Cy5 as the energy acceptor. Under 980 nm NIR laser excitation, UCNP@SiO_2 showed dual UCL emission bands in green and red parts of the visible region, respectively (as shown in Fig. S1). The absorption band of Cy5 is centered at 650 nm, which overlaps well with the red UCL emissions of UCNP@SiO_2, implying a FRET process between UCNP and Cy5. The amino-terminated Cy5-pep were conjugated with carboxyl modified UCNP@SiO_2 through covalent attachment. In the absence of caspase-9, the red UCL fluorescence signal of UCNP was quenched by Cy5, leading to a low UCL intensity. The Cy5 terminal of Cy5-pep can be released from the UCNP@SiO_2 surface when the LEHD fragment of Cy5-pep is cleaved by caspase-9, resulting in a recovery of red UCL emission. The recovery of red UCL emission is dependent on the activity of caspase-9, i.e., the higher activity of caspase-9 leads to stronger recovery of red UCL emission. Besides, the green UCL signal can be employed as an internal reference for ratiometric sensing because the green UCL emission of UCNP@SiO_2 remains unchanged before and after Cy5 releasing. Therefore, the accuracy of caspase-9 activity determination could be further improved using the UCL signal intensity ratio of red emission to green emission of UCNP (termed as R/G), i.e., higher R/G value means higher intracellular caspase-9 activity.

3.2. Characterization of UCNP@SiO_2@Cy5-pep

The OA capped $NaYF_4$: 20% Yb^{3+}, 2% Er^{3+}@$NaGdF_4$ UCNPs were synthesized for construction of the UCNP-based FRET sensing platform by a conventional solvothermal method because the UCL intensity of UCNP can be improved significantly by the core@shell structure (Wang et al., 2010b). A silica layer is coated on the hydrophobic OA capped UCNPs for transferring the UCNPs into aqueous medium, which is terminated by CTES to generate the carboxyl group on the particle surface (Liu et al. 2013a, 2013b). The carboxyl-terminated UCNP@SiO_2 are ready to be functionalized by biomolecules through the formation of amide bonds. The morphologies of as-prepared $NaYF_4$: Yb^{3+}, Er^{3+} UCNP, $NaYF_4$: Yb^{3+}, Er^{3+}@$NaGdF_4$ UCNP and UCNP@SiO_2 were characterized by TEM. As shown in Fig. 1, three kinds of UCNPs have uniform size and hexagonal structure. The average diameters of $NaYF_4$: Yb^{3+}, Er^{3+} and $NaYF_4$: Yb^{3+}, Er^{3+}@$NaGdF_4$ UCNP are 39 ± 2.8 nm and 48 ± 2.3 nm, respectively. After coated by silica shell, the average diameter of UCNP@SiO_2 reaches 55 ± 2.6 nm, indicating that the thickness of silica shell is about 3 nm. The corresponding HRTEM micrographs exhibit the highly crystalline nature of UCNPs (as shown in the inset of Fig. 1a-c). XRD patterns of $NaYF_4$: Yb^{3+}, Er^{3+} and $NaYF_4$: Yb^{3+}, Er^{3+}@$NaGdF_4$ UCNPs show that all the diffraction peaks can be attributed to the hexagonal phase of $NaYF_4$ (JCPDS NO. 16–0334) and $NaGdF_4$ (JCPDS NO. 27–0699) respectively (Fig. S2).

As shown in Fig. 2a, the UCNPs display three major UCL peaks at 521, 541, and 655 nm which are assigned to the energy transitions from $^2H_{11/2}$, $^4S_{3/2}$, and $^4F_{9/2}$ to $^4I_{15/2}$ of Er^{3+} ions, respectively (Li et al., 2009). As expected, the UCL emission of $NaYF_4$:Yb^{3+}, Er^{3+}@$NaGdF_4$ UCNPs is much stronger than that of $NaYF_4$:Yb^{3+}, Er^{3+} UCNPs since the outer $NaGdF_4$ shell can protect the migrating energy in Gd sublattice from trapping by surface quenchers. Due to increasing of surface defect by silica shell, the UCL intensity of UCNP@SiO_2 is decreased significantly, which is consistent with a previous report (Liu et al., 2014). After the conjugation of Cy5-pep, the red UCL intensity of UCNP@SiO_2 is further decreased obviously while the green UCL emission remains unaffected (as shown in Fig. 2b). The quenching efficiency of red UCL emission of UCNP@SiO_2 is increased by increasing the concentration of Cy5-pep in the reaction mixture while the concentration of UCNP@SiO_2 is kept as constant. The maximum quenching efficiency (~82.3%) is obtained when the mass ratio of Cy5-pep to UCNP@SiO_2 (R_m) is more than 0.08 (as shown in Fig. 2b). In the following experiments, all of used UCNP@SiO_2@Cy5-pep were synthesized at R_m of 0.08. The fluorescence decay curves of UCNP@SiO_2 and

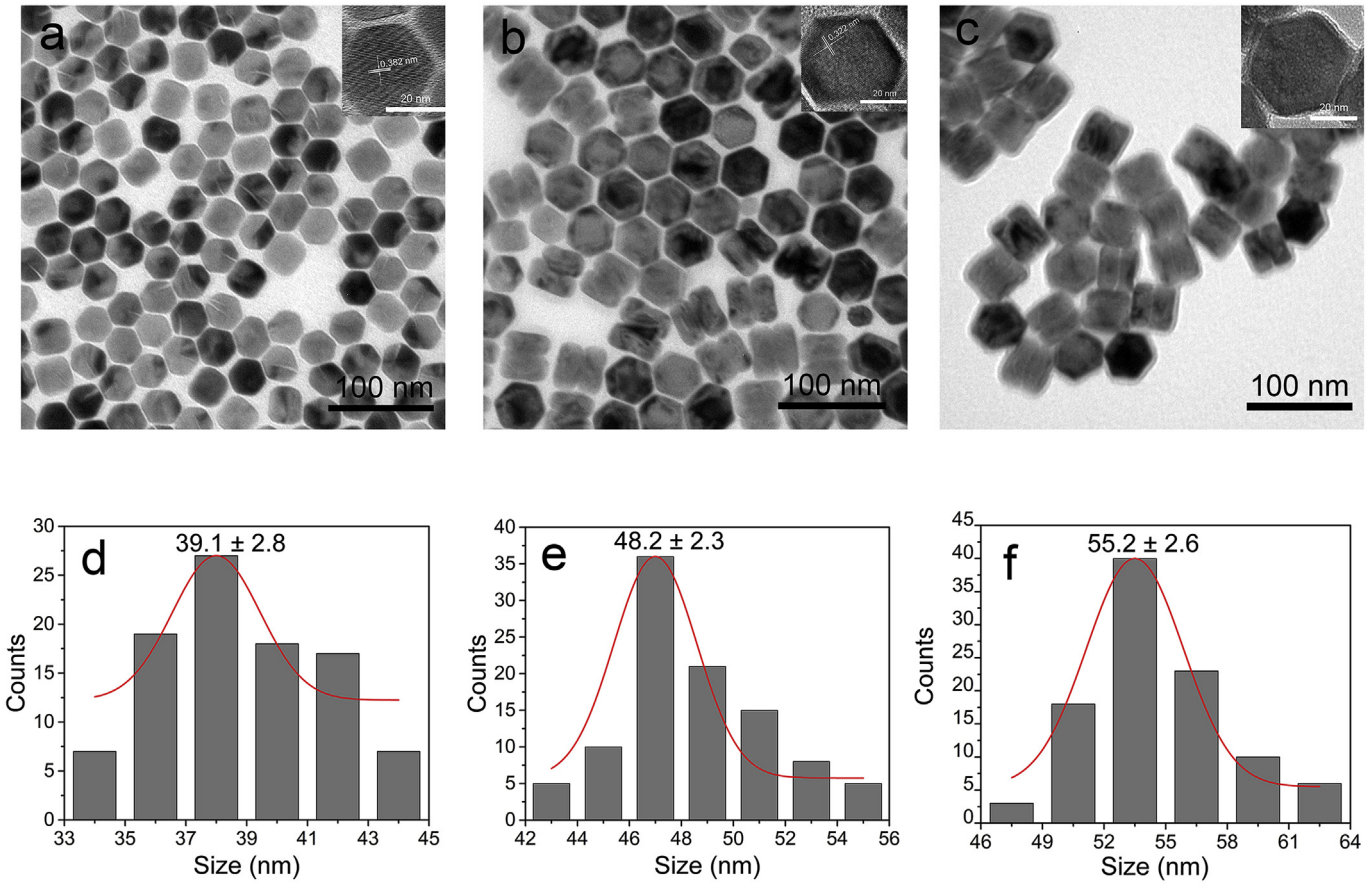

Fig. 1. TEM micrographs of (a) $NaYF_4$: Yb^{3+}, Er^{3+} UCNP, (b) $NaYF_4$: Yb^{3+}, Er^{3+}@$NaGdF_4$ UCNP, and (c) UCNP@SiO_2, respectively. The scale bars are 100 nm. The corresponding size and size distribution of the three types of NPs (d–f).

UCNP@SiO_2@Cy5-pep at 655 nm were also examined (as show in Fig. S3). The fluorescence lifetime showed a slight decrease, indicating the near-filed interaction between the UCNPs and Cy5. The UCNP@SiO_2 and UCNP@SiO_2@Cy5-pep were fully characterized by FTIR, XPS and TGA measurements. Compared with the FTIR spectrum of $NaYF_4$: Yb^{3+}, Er^{3+}@$NaGdF_4$ UCNP, the peaks at 1108 cm^{-1} and 812 cm^{-1} appear in the FTIR spectrum of UCNP@SiO_2, which are related to Si–O–Si groups (Lin et al., 2007; Wang et al., 2007). After conjugated with Cy5-pep, a new peaks at 1641 cm^{-1} is observed, which is associated with stretching vibration of amide bonds (as show in Fig. S4) (Tian et al., 2018). The result indicates that OA capped $NaYF_4$: Yb^{3+}, Er^{3+}@$NaGdF_4$ UCNPs are successfully coated by silica shell, and further conjugated with Cy5-pep. XPS results clearly show the presence of the element of Si in UCNP@SiO_2 and the element of N in UCNP@SiO_2@Cy5-pep, which also demonstrated the successful synthesis of UCNP@SiO_2@Cy5-pep (as show in Fig. S5). Moreover, TGA measurement reveals the total weight loss of UCNP@SiO_2@Cy5-pep is 19.7% compared to UCNP@SiO_2, providing further evidence for the surface coating of Cy5-pep (as shown in Fig. S6). In addition, the Zeta potential of UCNP@SiO_2@Cy5-pep is higher than that of UCNP@SiO_2 (as shown in Table S1) because the peptide CGRGGLEHDGGRK has relative high isoelectric points (PI = 9.0). The hydrodynamic diameters of UCNP@SiO_2 are significantly increased after the conjugation of Cy5-pep due to the interaction between the thin peptide layer and the water molecule layer nearby (as shown in Table S1). When UCNP@SiO_2@Cy5-pep were re-dispersed in different media (e.g. water, PBS, HEPES (pH = 7.4), 0.9 wt% NaCl, DMEM with/without FBS, L-15 with/without FBS), no aggregation was observed (Fig. S7), indicating the good monodispersity and colloidal stability of the as-prepared conjugates.

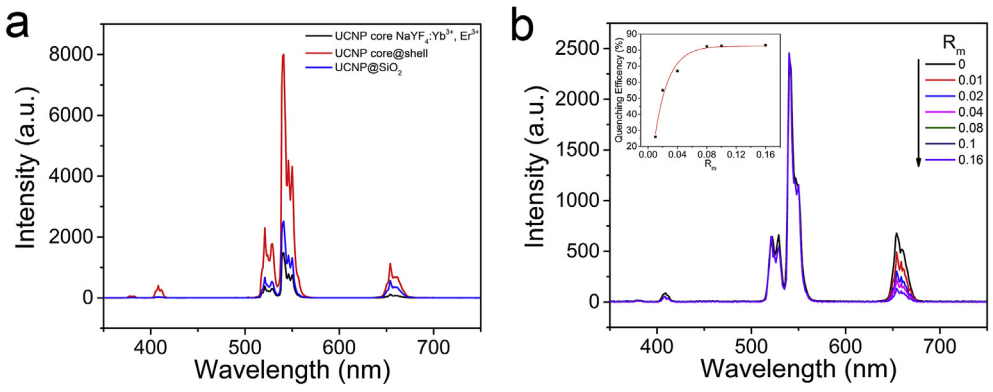

Fig. 2. (a) The UCL fluorescence spectra of $NaYF_4$: Yb^{3+}, Er^{3+} UCNP, $NaYF_4$: Yb^{3+}, Er^{3+}@$NaGdF_4$ UCNP, and UCNP@SiO_2, respectively. (b) The UCL fluorescence spectra of UCNP@SiO_2 and UCNP@SiO_2@Cy5-pep conjugates at different mass ratio of Cy5-pep to UCNP@SiO_2 (R_m) and the insert graph is the fluorescence quenching efficiency of UCNP@SiO_2@Cy5-pep conjugates at different R_m.

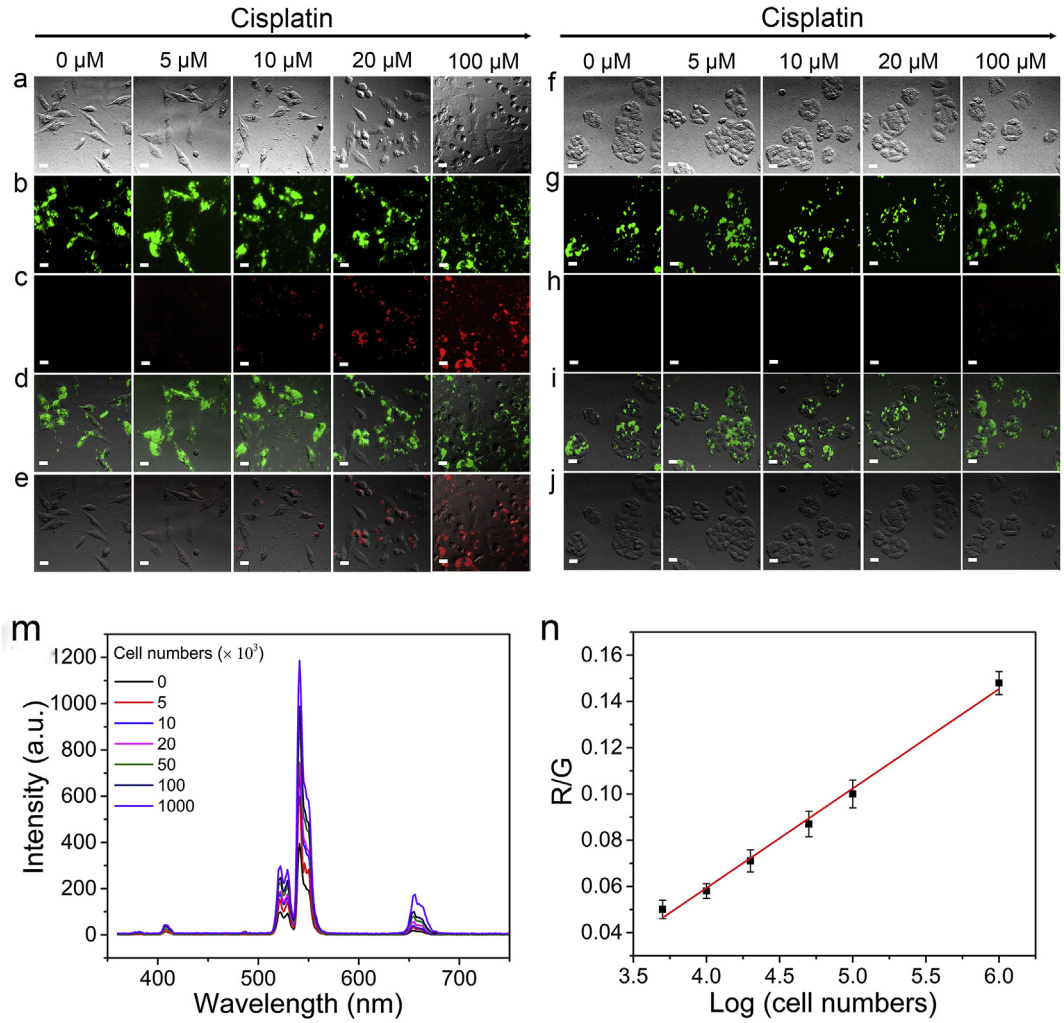

Fig. 3. UCL images of UCNP@SiO_2@Cy5-pep stained MG-63 cells (a-e), SW480 cells (f-j) treated with various concentrations of cisplatin for 12 h. The images are obtained from bright-field mode (a, f), UCL green channel (b, g), UCL red channel (c, h), merged images of bright-field and UCL green channel (d, i) and merged images of bright-field and UCL red channel (e, j) respectively. The scale bars are 20 μm. The UCL fluorescence spectra of UCNP@SiO_2@Cy5-pep stained various amounts of MG-63 cells which were treated with 100 μM cisplatin for 12 h (m) and the R/G values as a function of the logarithm of MG-63 cell numbers (n). (For interpretation of the references to color in this figure legend, the reader is referred to the Web version of this article.)

3.3. Intracellular caspase-9 activity detection

In this study, two kinds of cancer cells (MG-63 (human osteosarcoma cell) and SW480 (human colon cancer cell)) are arbitrarily selected to test the capability of UCNP@SiO_2@Cy5-pep for detection of caspase-9 activity in vitro. Before the detection of intracellular caspase-9 activity, the cytotoxicity of UCNP@SiO_2@Cy5-pep was investigated. After co-cultured with cells for 24 h, UCNP@SiO_2@Cy5-pep show a negligible cytotoxicity as high as the concentration of 200 μg mL^{-1} (as shown in Fig. S8). In this case, cisplatin, one of the most widely used anticancer drugs was employed as the inducer to activate intracellular caspase-9 since cisplatin can cause cancer cell death through triggering cell apoptosis. The intracellular caspase-9 activity was monitored by UCL imaging. As shown in Fig. 3, after incubating with UCNP@SiO_2@Cy5-pep in serum-free culture medium, both of MG-63 cells and SW480 cells exhibit strong green UCL emission, indicating that UCNP@SiO_2@Cy5-pep can be efficiently internalized by MG-63 cells and SW480 cells. In the presence of cisplatin, the red UCL emission of UCNP@SiO_2@Cy5-pep stained cells gradually enhanced along with increasing cisplatin concentration from 10 to 100 μM, while the green UCL emission of UCNP@SiO_2@Cy5-pep stained cells exhibits negligible change under same experimental conditions. At same concentration of cisplatin, the increasing of red UCL emission of UCNP@SiO_2@Cy5-pep stained MG-63 cells is much stronger than that of red UCL emission of UCNP@SiO_2@Cy5-pep stained SW480 cells. The result indicates that the intracellular caspase-9 activity level of MG-63 cells is increased significantly by the cisplatin. By the contrast, cisplatin exhibit weak effect on the intracellular caspase-9 activity level of SW480 cells. The intracellular caspase-9 activity of MG-63 cells was also determined by UCL spectroscopy (as seen from Fig. S9). The red UCL emission intensity of UCNPs is increased with increasing the concentration of cisplatin while the green UCL emission intensity of UCNPs keeps as constant, which coincides with the result of UCL imaging. The intracellular caspase-9 activity levels of MG-63 cells and SW480 cells were further measured by commercial caspase-9 activity colorimetric assay kit (as shown in Fig. S10). The result of commercial assay is in accordance with the result of UCNP@SiO_2@Cy5-pep. In addition, caspase-9 activities in different numbers of MG-63 cells were determined by a commercial caspase-9 activity colorimetric assay kit. According to obtained standard calibration curve of the kit (as shown in Fig. S11), the caspase-9 activity in 1×10^4 cells was equal to about 1 U mL^{-1} pure caspase-9. As shown in Fig. 3m, the red UCL emission intensity is gradually increased with the increasing of MG-63 cell numbers. And the R/G value of UCNPs is linear with the logarithm of MG-63 cell numbers within the range of 5×10^3 to 1×10^6 cells (i.e., 0.5–100 U mL^{-1} caspase-9) with a limit of detection (LOD) of 675 cells (i.e., 0.068 U mL^{-1} caspase-9).

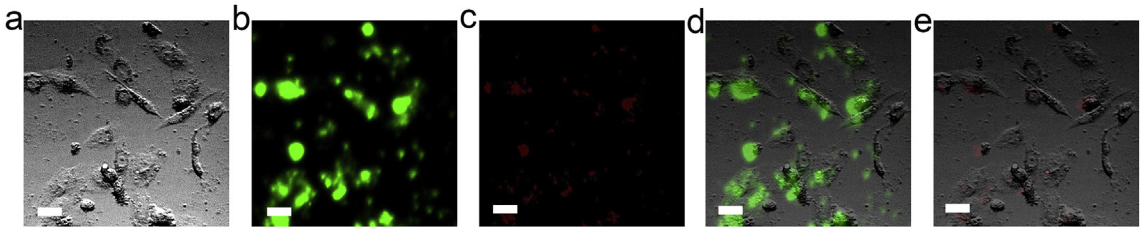

Fig. 4. UCL images of UCNP@SiO_2@Cy5-pep stained MG-63 cells treated with 100 μM cisplatin in the presence of Ac-LEHD-FMK. The images are obtained from bright-field mode (a), UCL green channel (b), UCL red channel (c), merged images of bright-field and UCL green channel (d) and merged images of bright-field and UCL red channel (e), respectively. The scale bars are 20 μm. (For interpretation of the references to color in this figure legend, the reader is referred to the Web version of this article.)

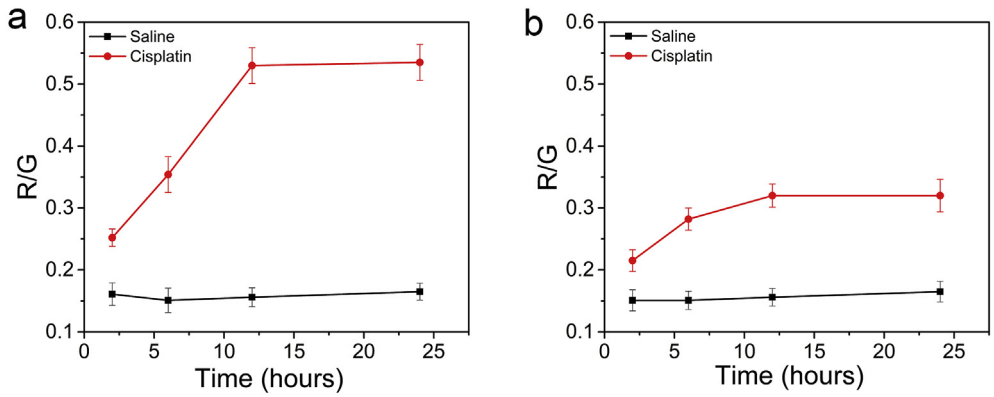

Fig. 5. Comparison between the MG-63 tumors (a) and SW480 tumors (b) treated with cisplatin and saline by the ratio of red emission with green emission of UCL (n = 3). (For interpretation of the references to color in this figure legend, the reader is referred to the Web version of this article.)

In the presence of cisplatin, the morphology of MG-63 cells is changed from the stretching/adhesive state to the shrinkage state/detached state with the increasing concentration of cisplatin, which demonstrates the occurrence of cisplatin-induced cell apoptosis. The SW480 cells shows negligible changes of morphology and adhesive behavior when the cells are treated by as high as 100 μM cisplatin. The results indicates that SW480 cells have strong anti-cisplatin capability. Furthermore, the MG-63 cells exhibit a viability of 82% with 5 μM cisplatin and a viability of 23% with 100 μM cisplatin, while SW480 cells still shows a viability of 75% with 100 μM cisplatin (as shown in Fig. S12). This phenomenon suggests that UCNP@SiO_2@Cy5-pep could be used to evaluate efficiency of anti-cancer drug through monitoring the intracellular caspase-9 activity level of cells.

In order to further validate that the red UCL emission recovery of UCNP@SiO_2@Cy5-pep is caused by eliminating FRET system through the cleavage of Cy5-pep by caspase-9, UCNP@SiO_2@Cy5-pep stained MG-63 cells were treated with 100 μM cisplatin plus 50 μM Ac-LEHD-FMK. As expected, the red UCL emission recovery of UCNP@SiO_2@Cy5-pep is suppressed significantly by the Ac-LEHD-FMK (as shown in Fig. 4). In addition, the Ac-LEHD-FMK shows no obvious cytotoxicity towards MG-63 cells (as shown in Fig. S13). The result further confirms the validity and practicability of the UCNP@SiO_2@Cy5-pep for intracellular caspase-9 detection.

3.4. In vivo caspase-9 activity detection

Examination of caspase-9 activity in vivo would provide a valuable parameter for therapeutic efficiency evaluation and drug screening since caspase-9 activation is triggered by apoptotic signaling events. The BALB/c mice bearing xenograft MG-63 tumor model and SW480 tumor model were established for testing the capability of UCNP@SiO_2@Cy5-pep to monitor caspase-9 activity in vivo. When the volumes of tumors reached about 40 mm^3, the MG-63 tumor-bearing mice or SW480 tumor-bearing mice were randomly divided into two groups, which were treated by cisplatin (5 mg kg^{-1} bodyweight) or saline through intratumoral injection, respectively. After cisplatin or saline treatment, the tumor-bearing mice were injected intravenously with 6 mg UCNP@SiO_2@Cy5-pep in 200 μL saline (0.9 wt% NaCl) through tail vein. The in vivo UCL signals of tumor sites were collected at different time points of post-injection (as shown in Figs. S14 and S15). Bright green UCL signals were observed at tumor sites of all mice after 1 h injection, indicating that UCNP@SiO_2@Cy5-pep were accumulated in the tumor tissue. The R/G values of cisplatin treated tumors are increased with the prolongation of time after injection, and saturated at 12 h post-injection, while the R/G values of saline treated tumors exhibits negligible changes (as shown in Fig. 5). In particular, the maximum R/G value of cisplatin treated MG-63 tumor is 1.7 times higher than that of cisplatin treated SW480 tumor. The result demonstrates that UCNP@SiO_2@Cy5-pep has the ability to detect caspase-9 activity in vivo.

3.5. In vivo toxicity evaluation

The healthy mice were intravenously injected with a single dose of UCNP@SiO_2@Cy5-pep and sacrificed at 30 days post-injection. The histology analysis demonstrates that there are negligible tissue damage and adverse effect of UCNP@SiO_2@Cy5-pep on major organs including heart, liver, spleen, lung, and kidneys (as shown in Fig. S16). The biosafety of UCNP@SiO_2@Cy5-pep was also examined by blood biochemistry assay. There was no significant difference in blood composition between healthy mouse and UCNP@SiO_2@Cy5-pep-treated mouse (as shown in Table S2). The results further confirmed the low toxicity of UCNP@SiO_2@Cy5-pep.

4. Conclusion

In summary, UCNP@SiO_2@Cy5-pep has been synthesized through conjugation of Cy5 modified caspase-9 peptide substrate on the UCNP

surface, which is used as a biocompatible FRET sensing platform for the detection of caspase-9 activity both in vitro and in vivo. The real-time monitoring of caspase-9 activity in vivo plays important role in diseases prognosis and anti-cancer drugs development. Considering the excellent FRET property, good colloidal stability and low cytotoxicity of as-prepared UCNP@SiO_2@Cy5-pep, it is very suitable for in real time monitoring of caspase-9 activity in vivo. In the proof of principle experiment, we demonstrated that the UCNP@SiO_2@Cy5-pep can be employed to distinguish cisplatin-mediated changes of intracellular caspase-9 activities in different cells. Moreover, the practicability of UCNP@SiO_2@Cy5-pep is examined by in vivo visualization of caspase-9 activities in cisplatin pretreated mouse-bearing tumors. UCNP@SiO_2@Cy5-pep could be served as a powerful sensing platform for bioanalytical and biomedical applications such as monitoring of apoptotic process and discovery of apoptosis-targeted drug and evaluation of anti-cancer drug efficacy.

Declarations of interest

None.

Acknowledgement

The authors would like to thank the National Natural Science Foundation of China (Grant no. 21775145) for financial support.

Appendix A. Supplementary data

Supplementary data to this article can be found online at https://doi.org/10.1016/j.bios.2019.111403.

References

Achatz, D.E., Ali, R., Wolfbeis, O.S., 2011. Luminescent chemical sensing, biosensing, and screening using upconverting nanoparticles. In: Prodi, L., Montalti, M., Zaccheroni, N. (Eds.), Luminescence Applied in Sensor Science. Springer-Verlag Berlin, Berlin, pp. 29–50.

Alonso-Cristobal, P., Vilela, P., El-Sagheer, A., Lopez-Cabarcos, E., Brown, T., Muskens, O.L., Rubio-Retama, J., Kanaras, A.G., 2015. Highly sensitive DNA sensor based on upconversion nanoparticles and graphene oxide. ACS Appl. Mater. Interfaces 7 (23), 12422–12429.

Chen, J., Zhao, J.X., 2012. Upconversion nanomaterials: synthesis, mechanism, and applications in sensing. Sensors 12 (3), 2414–2435.

Chen, H., Yuan, F., Wang, S., Xu, J., Zhang, Y., Wang, L., 2013. Aptamer-based sensing for thrombin in red region via fluorescence resonant energy transfer between $NaYF_4$:Yb,Er upconversion nanoparticles and gold nanorods. Biosens. Bioelectron. 48, 19–25.

Deveraux, Q.L., Roy, N., Stennicke, H.R., Van Arsdale, T., Zhou, Q., Srinivasula, S.M., Alnemri, E.S., Salvesen, G.S., Reed, J.C., 1998. IAPs block apoptotic events induced by caspase-8 and cytochrome c by direct inhibition of distinct caspases. EMBO J. 17 (8), 2215–2223.

Hakem, R., Hakem, A., Duncan, G.S., Henderson, J.T., Woo, M., Soengas, M.S., Elia, A., de la Pompa, J.L., Kagi, D., Khoo, W., Potter, J., Yoshida, R., Kaufman, S.A., Lowe, S.W., Penninger, J.M., Mak, T.W., 1998. Differential requirement for Caspase 9 in apoptotic pathways in vivo. Cell 94 (3), 339–352.

Hu, H., Xiong, L.Q., Zhou, J., Li, F.Y., Cao, T.Y., Huang, C.H., 2009. Multimodal-luminescence core-shell nanocomposites for targeted imaging of tumor cells. Chem. Eur J. 15 (14), 3577–3584.

Hurtley, S.M., 2016. Apoptosis, necrosis, and pyroptosis. Science 352 (6281), 48–50.

Jiang, S., Zhang, Y., 2010. Upconversion nanoparticle-based FRET system for study of siRNA in live cells. Langmuir 26 (9), 6689–6694.

Johnstone, R.W., Ruefli, A.A., Lowe, S.W., 2002. Apoptosis: a link between cancer genetics and chemotherapy. Cell 108 (2), 153–164.

Kerr, C.A., de la Rica, R., 2015. Photoluminescent nanosensors for intracellular detection. Anal. Methods. 7 (17), 7067–7075.

Li, P., Peng, Q., Li, Y., 2009. Dual-mode luminescent colloidal spheres from monodisperse rare-earth fluoride nanocrystals. Adv. Mater. 21 (19), 1945–1948.

Lin, C., Zhang, C., Lin, J., 2007. Phase transformation and photoluminescence properties of nanocrystalline ZrO_2 powders prepared via the Pechini-type sol-gel process. J. Phys. Chem. C 111 (8), 3300–3307.

Lin, F., Yin, B., Li, C., Deng, J., Fan, X., Yi, Y., Liu, C., Li, H., Zhang, Y., Yao, S., 2013. Fluorescence resonance energy transfer aptasensor for platelet-derived growth factor detection based on upconversion nanoparticles in 30% blood serum. Anal. Methods. 5 (3), 699–704.

Liu, F., He, X., Liu, L., You, H., Zhang, H., Wang, Z., 2013a. Conjugation of $NaGdF_4$ upconverting nanoparticles on silica nanospheres as contrast agents for multi-modality imaging. Biomaterials 34 (21), 5218–5225.

Liu, F., Zhao, Q., You, H., Wang, Z., 2013b. Synthesis of stable carboxy-terminated $NaYF_4$:Yb^{3+}, Er^{3+}@SiO_2 nanoparticles with ultrathin shell for biolabeling applications. Nanoscale 5 (3), 1047–1053.

Liu, B., Li, C., Yang, D., Hou, Z., Ma, P.a., Cheng, Z., Lian, H., Huang, S., Lin, J., 2014. Upconversion-LuminescentCore/mesoporous-silica-shell-Structured β-$NaYF_4$:Yb^{3+},Er^{3+}@SiO_2@mSiO_2 composite nanospheres: fabrication and drug-storage/release properties. Eur. J. Inorg. Chem. 2014 (11), 1906–1913.

MacFarlane, M., Cain, K., Sun, X.-M., Alnemri, E.S., Cohen, G.M., 1997. Processing/activation of at least four interleukin-1β converting enzyme–like proteases occurs during the execution phase of apoptosis in human monocytic tumor cells. J. Cell Biol. 137 (2), 469–479.

Mehmet, H., 2000. Apoptosis - caspases find a new place to hide. Nature 403 (6765), 29–30.

Mujumdar, R.B., Ernst, L.A., Mujumdar, S.R., Lewis, C.J., Waggoner, A.S., 1993. Cyanine dye labeling reagents - sulfoindocyanine succinimidyl esters. Bioconjug. Chem. 4 (2), 105–111.

Park, Y.I., Lee, K.T., Suh, Y.D., Hyeon, T., 2015. Upconverting nanoparticles: a versatile platform for wide-field two-photon microscopy and multi-modal in vivo imaging. Chem. Soc. Rev. 44 (6), 1302–1317.

Poreba, M., Szalek, A., Kasperkiewicz, P., Rut, W., Salvesen, G.S., Drag, M., 2015. Small molecule active site directed tools for studying human caspases. Chem. Rev. 115 (22), 12546–12629.

Prokhorova, E.A., Kopeina, G.S., Lavrik, I.N., Zhivotovsky, B., 2018. Apoptosis regulation by subcellular relocation of caspases. Sci. Rep. 8.

Qiao, X.-F., Zhou, J.-C., Xiao, J.-W., Wang, Y.-F., Sun, L.-D., Yan, C.-H., 2012. Triple-functional core-shell structured upconversion luminescent nanoparticles covalently grafted with photosensitizer for luminescent, magnetic resonance imaging and photodynamic therapy in vitro. Nanoscale 4 (15), 4611–4623.

Shi, J.Y., Tian, F., Lyu, J., Yang, M., 2015. Nanoparticle based fluorescence resonance energy transfer (FRET) for biosensing applications. J. Math. Chem. B 3 (35), 6989–7005.

Shieh, P., Jan, C.-R., Liang, W.-Z., 2019. The protective effects of the antioxidant N-acetylcysteine (NAC) against oxidative stress-associated apoptosis evoked by the organophosphorus insecticide malathion in normal human astrocytes. Toxicology 417, 1–14.

Sun, X.M., MacFarlane, M., Zhuang, J.G., Wolf, B.B., Green, D.R., Cohen, G.M., 1999. Distinct caspase cascades are initiated in receptor-mediated and chemical-induced apoptosis. J. Biol. Chem. 274 (8), 5053–5060.

Suzuki, M., Sakata, I., Sakai, T., Tomioka, H., Nishigaki, K., Tramier, M., Coppey-Moisan, M., 2015. A high-throughput direct fluorescence resonance energy transfer-based assay for analyzing apoptotic proteases using flow cytometry and fluorescence lifetime measurements. Anal. Biochem. 491, 10–17.

Thamizharasi, G., Sindhu, G., Veeravarmal, V., Nalini, N., 2019. Preventive effect of D-carvone during DMBA induced mouse skin tumorigenesis by modulating xenobiotic metabolism and induction of apoptotic events. Biomed. Pharmacother. 111, 178–187.

Tian, R., Zhang, H., Chen, H., Liu, G., Wang, Z., 2018. Uncovering the binding specificities of lectins with cells for precision colorectal cancer diagnosis based on multimodal imaging. Adv. Sci. 5 (6).

Tian, H., Liu, L., Li, Z., Liu, W., Sun, Z., Xu, Y., Wang, S., Liang, C., Hai, Y., Feng, Q., Zhao, Y., Hu, Y., Peng, J., 2019. Chinese medicine CGA formula ameliorates liver fibrosis induced by carbon tetrachloride involving inhibition of hepatic apoptosis in rats. J. Ethnopharmacol. 232, 227–235.

Vaux, D.L., Korsmeyer, S.J., 1999. Cell death in development. Cell 96 (2), 245–254.

Wang, F., Liu, J.H., Luo, Z.K., Zhang, Q.L., Wang, P.X., Liang, X., Li, C.H., Chen, J.Z., 2007. Effects of dimethyldiethoxysilane addition on the sol-gel process of tetraethylorthosilicate. J. Non-Cryst. Solids 353 (3), 321–326.

Wang, M., Mi, C.-C., Wang, W.-X., Liu, C.-H., Wu, Y.-F., Xu, Z.-R., Mao, C.-B., Xu, S.-K., 2009. Immunolabeling and NIR-excited fluorescent imaging of HeLa cells by using $NaYF_4$:Yb,Er upconversion nanoparticles. ACS Nano 3 (6), 1580–1586.

Wang, F., Banerjee, D., Liu, Y.S., Chen, X.Y., Liu, X.G., 2010a. Upconversion nanoparticles in biological labeling, imaging, and therapy. Analyst 135 (8), 1839–1854.

Wang, F., Wang, J.A., Liu, X.G., 2010b. Direct evidence of a surface quenching effect on size-dependent luminescence of upconversion nanoparticles. Angew. Chem. Int. Ed. 49 (41), 7456–7460.

Wang, C., Li, X., Zhang, F., 2016. Bioapplications and biotechnologies of upconversion nanoparticle-based nanosensors. Analyst 141 (12), 3601–3620.

Wu, S., Duan, N., Li, X., Tan, G., Ma, X., Xia, Y., Wang, Z., Wang, H., 2013. Homogenous detection of fumonisin B-1 with a molecular beacon based on fluorescence resonance energy transfer between $NaYF_4$: Yb, Ho upconversion nanoparticles and gold nanoparticles. Talanta 116, 611–618.

Yuan, F., Chen, H., Xu, J., Zhang, Y., Wu, Y., Wang, L., 2014. Aptamer-based luminescence energy transfer from near-infrared-to-near-infrared upconverting nanoparticles to gold nanorods and its application for the detection of thrombin. Chem. Eur J. 20 (10), 2888–2894.

Zheng, W., Huang, P., Tu, D., Ma, E., Zhu, H., Chen, X., 2015. Lanthanide-doped upconversion nano-bioprobes: electronic structures, optical properties, and biodetection. Chem. Soc. Rev. 44 (6), 1379–1415.

Zhu, X., Su, Q., Feng, W., Li, F., 2017. Anti-Stokes shift luminescent materials for bioapplications. Chem. Soc. Rev. 46 (4), 1025–1039.